Journal of Structural Chemistry. Vol. 56, No. 6, pp. 1112-1117, 2015.

STUDY OF THE STRUCTURAL FEATURES OF NONSTOICHIOMETRIC $SrCo_{0.8-x}Fe_{0.2}W_xO_{3-\delta}$ ($0 < x < 0.1$) PEROVSKITES

E. V. Artimonova[1], O. A. Savinskaya[1], I. V. Belenkaya[1], and A. P. Nemudry[1,2]

UDC 544.016.5:544.012:544.022.22

The work studies a partial tungsten substitution for cobalt in the structure of nonstoichiometric $SrCo_{0.8}Fe_{0.2}O_{3-\delta}$ (SCF) perovskite with mixed oxygen electron conductivity. It is shown that samples of the composition $SrCo_{0.8-x}Fe_{0.2}W_xO_{3-\delta}$ (SCFW) at $x \geq 0.03$ undergo the endotaxial phase separation with the formation of nanosized domains with a structure of ordered Sr_2CoWO_6 double perovskite, which are distributed in the matrix of nonstoichiometric $SrCo_{0.8-x}Fe_{0.2}W_xO_{3-\delta}$ perovskite. For the materials with $0.02 < x < 0.1$, a decrease in the oxygen stoichiometry is accompanied by nanostructuring of the matrix: the formation of nanosized domains in which oxygen vacancies are ordered with the formation of the brownmillerite-like structure.

DOI: 10.1134/S002247661506013X

Keywords: nonstoichiometric perovskites, nanostructuring, ceramic membranes.

INTRODUCTION

Nonstoichiometric oxides exhibiting mixed oxygen ionic and electronic conductivity find wide application as oxygen permeable membranes used to separate oxygen and obtain the synthesis gas, as oxygen sorbents for oxygen storage and transportation, to purify gases from oxygen impurities, to produce electrode materials for solid-oxide fuel cells (SOFCs) [1]. According to the literature data, cobaltites and ferrites with the perovskite structure, among which perovskites with the composition $SrCo_{0.8}Fe_{0.2}O_{3-\delta}$ (SCF) and $Ba_{0.5}Sr_{0.5}Co_{0.8}Fe_{0.2}O_{3-\delta}$ (BSCF) are most active, have the highest oxygen conductivities. However, these materials have disadvantages: phase transformations in the range of working temperatures, which decrease their mechanical strength; low chemical stability at a reduced partial pressure of oxygen; and their degradation in the presence of CO_2 [2]. For modifying the functional properties of membrane materials, we have proposed a partial replacement of *B* cations (Co/Fe) by highly charged Nb/Ta (V) and Mo/W (VI) cations [3-6]. In [7], it was shown that new nonstoichiometric $SrCo_{0.8-x}Fe_{0.2}W_xO_{3-\delta}$ (SCFW) oxides are promising materials to design oxygen permeable membranes and cathodes for SOFCs. The W^{6+} cation substitution for cobalt cations in the structure of SCF gives the possibility to decrease the working temperature of membrane materials owing to the suppression of perovskite-brownmillerite structural transition and enhanced thermomechanical stability at $T < 700$°C and $p_{O_2} < 0.06$ at. The introduction of W^{6+}

[1]Institute of Solid State Chemistry and Mechanochemistry, Siberian Branch, Russian Academy of Sciences, Novosibirsk, Russia; nemudry@solid.nsc.ru. [2]Novosibirsk National Research State University, Russia. Translated from *Zhurnal Strukturnoi Khimii*, Vol. 56, No. 6, pp. 1165-1170, November-December, 2015. Original article submitted September 30, 2014; revised November 7, 2014.

cations in the SCF structure significantly increases oxygen flows through the SCFW membranes in the atmosphere containing CO_2. This work comprehensively studies the effect of highly charged W^{6+} cation substitution for cobalt cations in the structure of $SrCo_{0.8}Fe_{0.2}O_{3-\delta}$ (SCF) on the structure of new nonstoichiometric SCFW perovskites, being an essential stage in the design of membrane materials and regulation of their functional properties.

EXPERIMENTAL

The SCFW compounds under consideration were synthesized by a ceramic method according to the technique described in detail in [8]. In the last stage, the pallets were annealed in the air at T = 1300-1430°C for 6 h. In order to change the oxygen stoichiometry of the samples, they were treated in different ways: slow cooling in a furnace, sample annealing at 950°C in the dynamic vacuum ($p_{O_2} \sim 10^{-5}$ at) with subsequent sample quenching to room temperature.

To determine the phase composition of SCFW perovskites, X-ray diffraction was used. The measurements were performed on a Bruker D8 Advance diffractometer (CuK_α radiation) using a Lynx Eye high-speed detector. The phase analysis was carried out using the ICDD PDF-4+ powder diffraction database (2011).

To examine the microstructure of the compounds under consideration, we used high-resolution transmission electron microscopy (HRTEM). The HRTEM study of the samples was performed on a JEM-2010 electron microscope (accelerating voltage 200 kV, resolving power 1.4 Å). The local elemental composition analysis of the samples was performed on an EDAX "Phoenix" energy dispersive spectrometer with a Si(Li) detector and an energy resolution below 130 eV. The data were processed using the DigitalMicrograph software.

The short-range structure, oxidation states of iron ions and their coordination in the compounds under consideration were studied using Mössbauer spectroscopy. The chemical shifts were determined relative to α-Fe. Percentage of iron with different oxidation states and coordination was calculated from the ratio of the areas of peaks in the spectra.

RESULTS AND DISCUSSION

Fig. 1 shows the diffraction patterns of the SCFW samples slowly cooled in the air. According to our data, at $x \geq 0.03$, the synthesis leads to the formation of a two-phase system consisting of nonstoichiometric $SrCo_{0.8-x}Fe_{0.2}W_xO_{3-\delta}$ oxide with the cubic $Pm\bar{3}m$ structure ($SrCo_{0.8}Fe_{0.2}O_{3-\delta}$, PDF No. 01-075-7788) and ordered Sr_2CoWO_6 double perovskite with the tetragonal $I4/m$ structure (PDF No. 04-014-6275). When the dopant content $x < 0.03$, the diffraction peaks monotonically shift in the small angle region, with a respective increase in the unit cell parameters of the phase of nonstoichiometric $SrCo_{0.8-x}Fe_{0.2}W_xO_{3-\delta}$ oxide (Fig. 2). This indicates that tungsten ions isomorphically substitute for cobalt

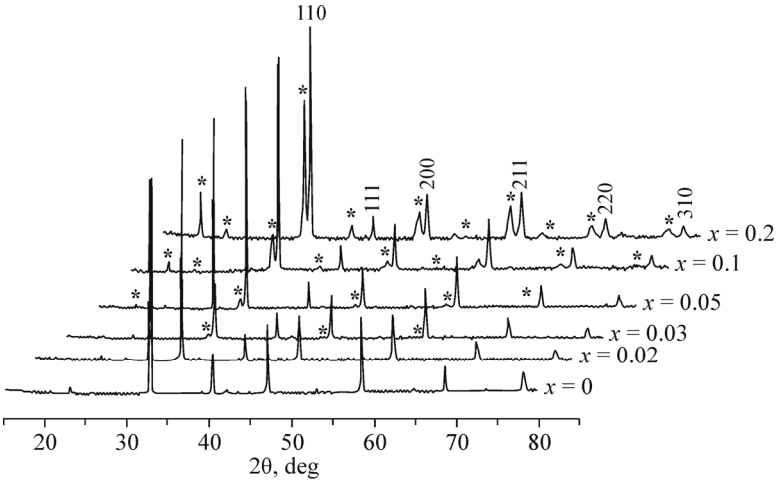

Fig. 1. Diffraction patterns of the SCFW samples slowly cooled in the air (the phase of Sr_2CoWO_6 double perovskite is denoted by *).

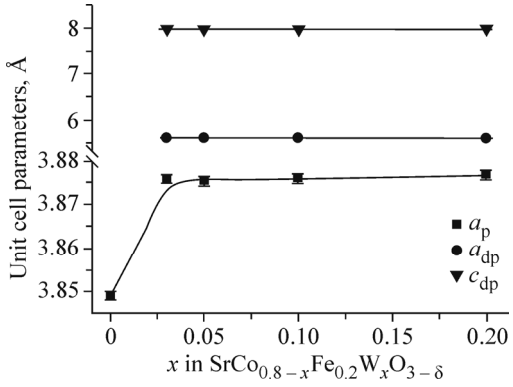

Fig. 2. Dependence of the unit cell parameters for the SCFW samples slowly cooled in the air on the dopant content (indices "p" and "dp" refer to the phases of cubic perovskite and double perovskite respectively).

ions in the crystal structure of perovskite, while the plateau of the curve at $x \geq 0.03$ means that the solubility limit of tungsten ions in the initial matrix is reached. An increase in the structural parameters of the $SrCo_{0.8-x}Fe_{0.2}W_xO_{3-\delta}$ phase with the tungsten content ($0 < x < 0.03$) is due to the fact that the excess positive charge of the dopant is compensated by a decrease in the oxidation state of B (Co/Fe) cations ($B^{4+} \rightarrow B^{3+}$) and an increase in their radii [8]. An increase in the dopant content in the SCFW samples ($x \geq 0.03$) is accompanied by an increase in the intensity of the reflections characterizing the phase of Sr_2CoWO_6 double perovskite.

The formation of a heterogeneous system was demonstrated using HRTEM (Fig. 3). The data in Fig. 3 show that the sample with the chemical composition $SrCo_{0.75}Fe_{0.2}W_{0.05}O_{3-\delta}$ has a complex microstructure: it contains nanosized domains with a periodicity $d \sim 4.5$ Å distributed in the matrix with interplanar distances $d \sim 3.8$ Å. According to the data of the local elemental composition analysis, area (*2*) is enriched with tungsten cations, and the ratio between the Sr, Co, W cations is about 2:1:1 respectively. Based on the cation ratio calculated from the elemental analysis data, area (*1*) corresponds to nonstoichiometric SCFW oxide with the tungsten content of approximately 2%. The diffraction pattern in Fig. 3*a* obtained by the Fourier transformation of area (*1*) corresponds to the [011] projection of the cubic $Pm\bar{3}m$ structure of perovskite. After indexing performed by means of the ICDD PDF-4+ database (2011), the diffraction pattern corresponding to area (*2*) was assigned to ordered double perovskite that has the monoclinic $P2_1/n$ structure (PDF No. 04-014-7598). According to the electron microscopy data, the typical sizes of the domains with the composition $SrCo_{0.8-x}Fe_{0.2}W_xO_{3-\delta}$ and Sr_2CoWO_6 are >100 nm and 20 nm respectively. It is difficult to estimate the domain size of double perovskite from the diffraction data due to a low reflection intensity and the overlap of the diffraction peaks of the tetragonal $I4/m$ structure. According to the analysis of the matrix reflection width on the basis of $SrCo_{0.8-x}Fe_{0.2}W_xO_{3-\delta}$ perovskite, the domains are >100 nm in size, which agrees with the microscopy data.

Disagreement between the X-ray diffraction and electron microscopy data characterizing the structure of double perovskite is likely to be due to that the Sr_2CoWO_6 compound is a mixture of the monoclinic and tetragonal crystal structures. The literature data describing the structure of double perovskite are rather contradictory. In [9], Sr_2CoWO_6 double perovskite was assigned to a tetragonal structure. In the later study [10], the detailed structural investigation of Sr_2CoWO_6 by synchrotron radiation and neutron diffraction methods showed that at room temperature the structure of this compound could be represented as a mixture of the monoclinic ($P2_1/n$) and tetragonal ($I4/m$) crystal structures. Therewith, the ordered alternation of Co and W cations in the octahedral positions are common for different proposed crystal structures, and changes in the symmetry are due to the rotations of the octahedra [10].

Therefore, the ceramic synthesis of SCFW ($x \geq 0.03$) oxides involves the endotaxial growth of nanosized domains of ordered double perovskite distributed in the matrix of nonstoichiometric cubic perovskite. The formation of an endotaxial

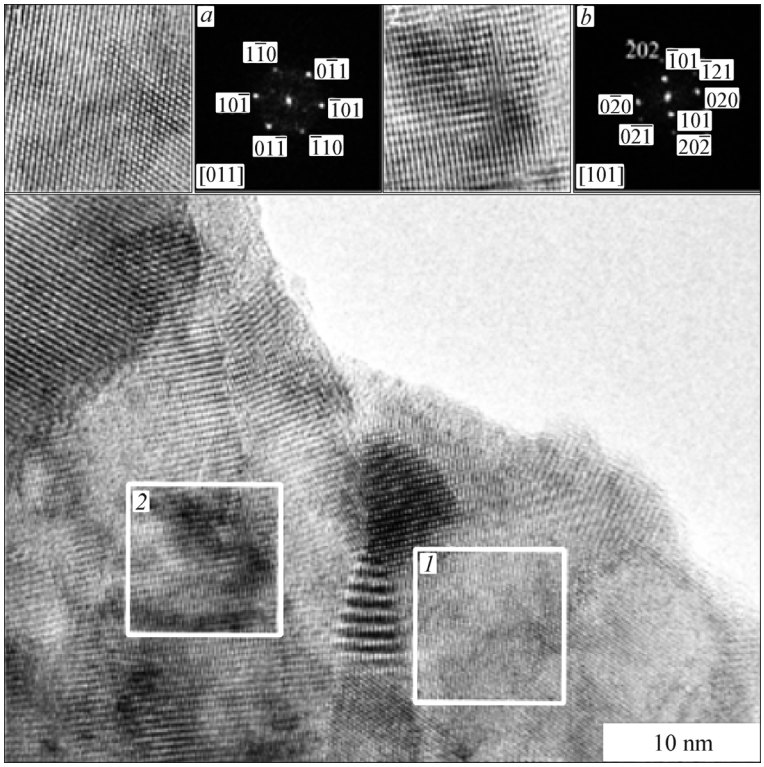

Fig. 3. Transmission electron microscopy data for SCFW (x = 0.05) and the respective diffraction patterns (*a*) and (*b*) obtained by the Fourier transformation of marked areas (*1*) and (*2*).

composite, when Mo^{6+} cations substitute for cobalt in $Ba_{0.5}Sr_{0.5}Co_{0.8}Fe_{0.2}O_{3-\delta}$, was previously demonstrated in [11]. The authors showed that the system separation with the formation of domains based on nonstoichiometric and double perovskites and the combination of the specific properties of these phases increased the stability and enhanced transportation characteristics of the cathode materials [11].

To get an insight into the state of the membrane material with respect to a low partial pressure of oxygen, we measured the diffraction patterns of vacuum-quenched SCFW oxides (Fig. 4). According to the literature data [12], the

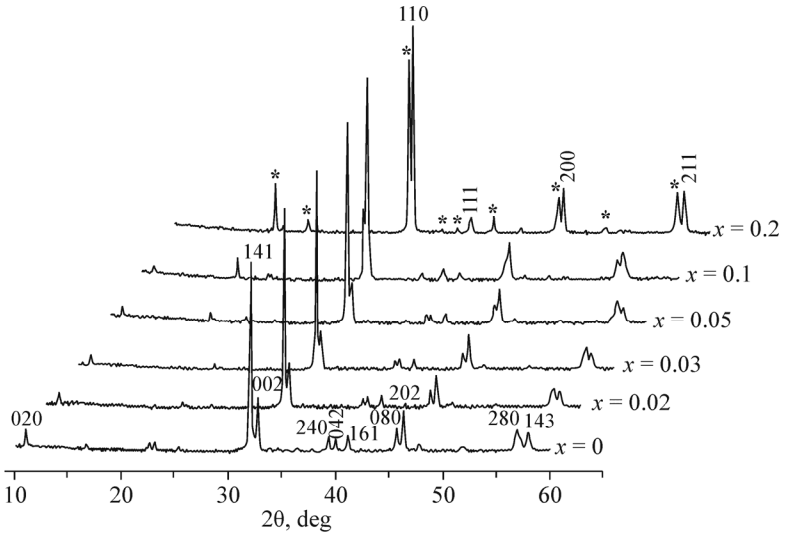

Fig. 4. Diffraction patterns of the vacuum-quenched SCFW samples (the additional phase of Sr_2CoWO_6 double perovskite is denoted by *****).

annealing and vacuum quenching of SCF perovskite leads to a structural transition and the formation of the vacancy-ordered orthorhombic brownmillerite structure (PDF No. 01-082-2446).

The structural analysis by the Rietveld method revealed that an increase in the dopant content resulted in the transformation of the orthorhombic *Ibmm* brownmillerite structure to the cubic $Pm\bar{3}m$ perovskite structure. Note that the ($Ibmm \rightarrow Pm\bar{3}m$) structural transformation occurs through the formation of a specific diffraction pattern for the samples with $x = 0.05$, 0.1; the X-ray diffraction patterns are characterized by the presence of intense main reflections indexed in the cubic unit cell of perovskite and by the additional diffuse peaks. Therewith, all reflections can be indexed in an orthorhombic unit cell with the parameters $a_b = c_b = \sqrt{2a_c}$ and $b_b = 4a_c$. An increase in the tungsten content leads to a decrease in the intensity of the diffuse peaks until their complete blurring in the background ($x = 0.2$). These diffraction phenomena were observed for a number of nonstoichiometric perovskites based on strontium ferrite and cobaltite and were shown to be associated with the formation of nanosized 90° domains of the brownmillerite structure [5, 13-15].

An increase in the dopant concentration results in a decrease in the domain/twin size (from 100 nm to 55 nm), which, in our case, is evidenced by the broadening of the reflections, for example, the (020) reflection, until their complete blurring in the background ($x = 0.2$). Since the domains are joined coherently, this leads to a convergence of the structural parameters (Fig. 5) near the interfaces. Consequently, when the density of domain boundaries is high, the orthorhombic distortions disappear, and for the sample with $x = 0.2$, the brownmillerite structure with the parameters $a_b/\sqrt{2} = b_b/4 = c_b/\sqrt{2}$ forms in the domains.

In order to confirm the hypothesis about the formation of a specific microstructure consisting of brownmillerite-type domains, we studied the short-range structure, the oxidation state of iron ions and their coordination in the considered compounds using Mössbauer spectroscopy. According to our data (Table 1), the spectra of the sample consist of two magnetically ordered sextets associated with Fe^{3+} ions in the octahedral and tetrahedral positions (in the 1:1 ratio) typical of the brownmillerite structure. An increase in the dopant content in SCFW leads to an increase in the coordination of iron atoms to compensate the excess positive charge, which is reflected in line broadening and a change in the component ratio in the spectra (Table 1).

CONCLUSIONS

A partial replacement of cobalt cations in the structure of SCF by highly charged W^{6+} cations ($x \geq 0.03$) on slow cooling in the air leads to the endotaxial growth of nanosized domains of ordered Sr_2CoWO_6 double perovskite distributed in the matrix of nonstoichiometric $SrCo_{0.8-x}Fe_{0.2}W_xO_{3-\delta}$ perovskite. A decrease in the oxygen stoichiometry is accompanied by the nanostructuring of the matrix: the formation of ~50 nm domains, in which oxygen vacancies are ordered, which is typical of the brownmillerite-like structure.

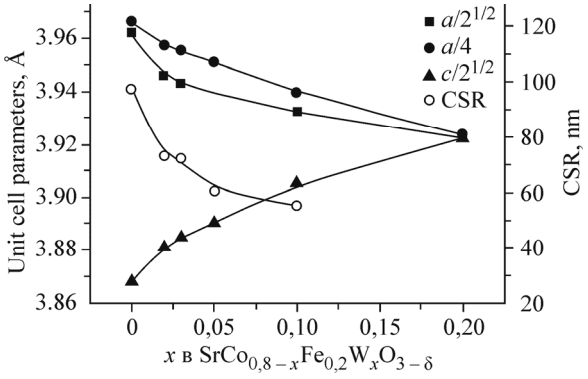

Fig. 5. Dependence of the specified unit cell parameters and CSR for the vacuum-quenched SCFW samples on the dopant content.

TABLE 1. Mössbauer Parameters for the Vacuum-Quenched SCFW Samples

x in SCFW	N	Iron charge and coordination	δ, mm/s	ε, mm/s	H, T	Content, %
$x = 0$	1	Fe^{3+} (O)	0.35	–0.34	47.57	51
	2	Fe^{3+} (T)	0.16	0.16	43.33	49
$x = 0.02$	1	Fe^{3+} (O)	0.34	–0.34	47.42	48
	2	Fe^{3+} (T)	0.16	0.18	41.67	52
$x = 0.03$	1	Fe^{3+} (O)	0.34	–0.33	47.60	50
	2	Fe^{3+} (T)	0.17	0.18	41.68	50
$x = 0.05$	1	Fe^{3+} (O)	0.32	–0.25	47.42	55
	2	Fe^{3+} (T)	0.18	0.16	42.28	45
$x = 0.1$	1	Fe^{3+} (O)	0.34	–0.25	48.56	57
	2	Fe^{3+} (T)	0.20	0.16	42.56	40
	3	Fe^{4+} (P)	0.16			3

δ, ε, H are the chemical shift, quadrupole splitting, magnetic field respectively. Symbols (O), (T), (P) correspond to the iron ions with the coordination numbers 6 (octahedron), 4 (tetrahedron), 5 (tetragonal pyramid) respectively.

The formation of a microheterogeneous system, as we have previously shown in [15], can cause the enhancement of transportation and thermomechanical properties of membrane and electrode materials. The conditions for the existence of microdomain texture of the SCFW materials at high temperatures and different p_{O_2} will be considered in subsequent studies.

The work was supported by RFBR (No. 14-03-31240).

REFERENCES

1. J. Sunarso, S. Baumann, J. M. Serra, et al., *J. Membr. Sci*., **320,** 13 (2008).
2. Z. Shao, G. Xiong, J. Tong, et al., *Sep. Purif. Technol*., **25,** 419 (2001).
3. I. A. Starkov, A. S. Kozhemyachenko, S. F. Bychkov, et al., *Bull. Russ. Acad. Sci.: Phys*., **74,** 1059 (2010).
4. I. L. Zhogin, A. P. Nemudry, P. V. Glyanenko, et al., *Catal. Today*, **118,** 151 (2006).
5. O. Savinskaya and A. Nemudry, *J. Solid State Electrochem*., **15,** 269 (2011).
6. M. P. Popov, I. A. Starkov, S. F. Bychkov, et al., *J. Membr. Sci*., **469,** 88 (2014).
7. E. V. Artimonova, O. A. Savinskaya, and A. P. Nemudry, *Dokl. Phys. Chem*., **465,** 295 (2015).
8. O. A. Savinskaya, A. P. Nemudry, A. N. Nadeev, et al., *Solid State Ionics*, **179,** 1076 (2008).
9. M. C. Viola, M. J. Martinez Lope, J. A. Alonso, et al., *Chem. Mater*., **15,** 1655 (2003).
10. Q. Zhou, B. J. Kennedy, and M. M. Elcombe, *J. Solid State Chem*., **180,** 541 (2007).
11. A. Demont, R. Sayers, and M. A. Tsiamtsouri, *J. Am. Chem. Soc*., **135,** 10114 (2013).
12. H. Kruidhof, H. J. M. Bouwmeester, R. H. E. Doorn, et al., *Solid State Ionics*, **63-65,** 816 (1993).
13. N. Nakayama, M. Takano, S. Inamura, et al., *J. Solid State Chem*., **71,** 403 (1987).
14. F. Lindberg, G. Svensson, S. Ya. Istomin, et al., *J. Solid State Chem*., **177,** 1592 (2004).
15. A. A. Markov, O. A. Savinskaya, M. V. Patrakeev, et al., *Solid State Chem*., **182,** 799 (2009).